IAC-10-C1.1.9

ELECTROSTATIC FORCE MODEL FOR TERRESTRIAL EXPERIMENTS ON THE COULOMB TESTBED

C.R. Seubert
University of Colorado at Boulder, USA, carl.seubert@colorado.edu

H. Schaub
University of Colorado at Boulder, USA, hanspeter.schaub@colorado.edu

Coulomb formation flight is a concept that utilizes the controllable electrostatic forces between charged spacecraft to maintain desired separation distances. The one-dimensional, near friction-less Coulomb testbed is designed and developed specifically to investigate the intricacies of charge production for this relative motion control. To perform experimental tests with low magnitude Coulomb forces the identification and mitigation of disturbances is undertaken. A terrestrial Coulomb force model that includes electrostatic influences for close finite spheres and induced charges is developed. Based on testbed conditions, this new force model differs from the previously used point charge force model by as much as 380%. The new model is verified with numerical solutions and then compared to testbed experimental results and shown to match well. Fundamental knowledge of electrostatic interactions is required for Coulomb force production and directly applies to the testbed as well as the spacecraft concept.

I. INTRODUCTION

There is a growing demand for the application of spacecraft formations to scientific, military, and commercial space missions. Applications using closely operating formations of spacecraft include remote sensing, situational awareness, interferometry, and cooperative/uncooperative rendezvous. Not only is it desirable to utilize the smaller, lighter spacecraft that comprise a formation, but such a distributed network also offers system redundancy. Furthermore, certain missions can be enhanced using a spacecraft formation; in the field of remote sensing, sensor resolution and observation power can be increased by utilizing spacecraft separated by tens to hundreds of meters[1,2]. Operational autonomous formation flight missions include PRISMA[3], but there are also future missions, such as NASA's proposed terrestrial planet finder[4] and stellar imager[5] concepts and ESA's Darwin[6] mission, that will continue to expand the technology and capabilities of spacecraft formation flight.

Formations requiring separation distances on the order of tens of meters introduce the necessity for highly accurate relative position sensing and determination as well as frequent and, in some cases, continuous micro-Newton-level manoeuvres. For very closely spaced spacecraft formations using conventional chemical or electric thrusters, there is also the concern for plume contamination on instrument and spacecraft surfaces. These challenges can be mitigated through the application of electrostatic (Coulomb) forces for spacecraft formation relative motion control. Using electrostatic forces, the relative spacecraft dynamics can be precisely controlled[7,8]. Furthermore, plume impingement is alleviated with the near propellant-less thrusting mechanism.

Coulomb formation flight (CFF) is a concept that utilizes electrostatic forces to maintain a formation of spacecraft. With each spacecraft charged to low-kilovolt level potentials and separations on the order of tens of meters, micro- to milli-Newton-level attractive and repulsive Coulomb forces are achievable[8]. These attractive and repulsive forces are envisioned to control the relative motion of spacecraft. These craft could also utilize traditional impulsive thrusters to perform non-line-of-sight and inertial manoeuvres. A conceptual example of a two-spacecraft formation doing collaborative sensing that uses Coulomb forces for separation control is shown in Fig. 1. In order to provide accurate formation control forces, the CFF concept requires precise potential control. Fortunately, charge control devices are space-based technologies that demonstrate voltage-level potential control on the ESA CLUSTER[9] and Geotail[10] missions.

In addition to mitigating several close-proximity operational concerns, natural charging that occurs from interaction with the space environment can be built upon, modified and maintained with the charge emission device[11,12]. Geosynchronous Earth Orbit (GEO) spacecraft, such as SCATHA, have been developed to study natural charging and potential control[13].

At GEO spacecraft can naturally charge to kilovolt potentials, such as the ATS-6 spacecraft that measured natural charging as low as -19 kV[14]. Through intended

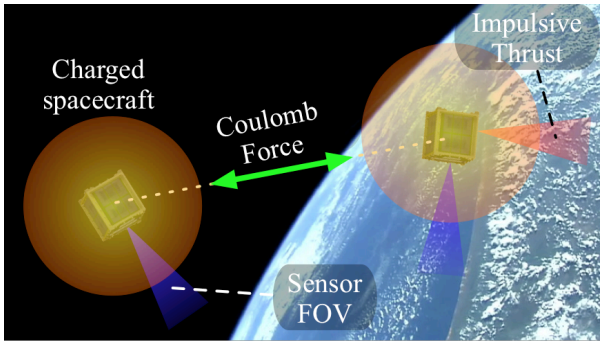

Fig. 1: Conceptual illustration of a two spacecraft formation performing collaborative sensing with the use of Coulomb forces for separation control.

design and with the use of a charge emission device charging to this degree can be safely managed and controlled. SPEAR-I demonstrated that charging beyond 40 kV is possible in the dense plasma of Low Earth Orbit (LEO)[15,16].

One of the primary benefits of Coulomb formation control is the increase in efficiency over conventional electric spacecraft control techniques. A charge control device requires only Watt-levels of power to reach desired potentials. Additionally, Coulomb formation control emits electrons or ions, resulting in almost negligible manoeuvre fuel costs[8,17].

Due to natural shielding from the space environment, spacecraft formations with Coulomb control are to be placed in GEO and high altitude orbits where the plasma is hot and sparse, reducing the partial shielding of Coulomb forces. At these high altitudes, the upper limit of separation baselines for effective Coulomb control is 100 meters[8].

Analytic research into the CFF concept has substantially grown since its inception in 2002[8]. These theoretical studies include static equilibrium orbit configurations[18,19]. These relative equilibrium solutions are naturally unstable, so feedback control is necessary. Control development is being pursued for two spacecraft with fixed separation distances[20], three craft[21,22,23] as well as for generic spacecraft numbers[24]. CFF studies have also expanded to asteroid deflection applications[25] and to tethered spacecraft formations[17]. For a tethered application the charged spacecraft provides an inflationary force to ensure the short-length tether remains in tension under any orbit alignment[17].

To build upon these theoretical studies and fully expand the opportunities of the CFF concept, the next fundamental step necessitates terrestrial hardware implementation. Through laboratory development the intricacies of Coulomb force production and charging characteristics can be appreciated and a wealth of knowledge gained. A terrestrial testbed for Coulomb controlled relative motion studies is sought.

There are existing terrestrial testing platforms dedicated to spacecraft formation flight concepts. These include NASA's formation control testbed[26] and flat floor testbed[27]. These testbeds are designed for large spacecraft systems with well-known dynamics and relative motion actuation devices with Newton-level thrusting. On a smaller scale, the MIT SPHERES formation flight program features a low-friction flatbed. The 4 kg SPHERES spacecraft feature thrusters with a force magnitude as great as 110 mN; however this was insufficient thrust to completely overcome the friction and disturbances present on the testbed[28]. For the terrestrial Coulomb testbed, the electrostatic forces are on the order of tens of mN, highlighting the need for a testbed with rigorous disturbance mitigation.

Due to the relatively low Coulomb force magnitudes, there is a need to have an extremely low disturbance environment to perform charged relative motion experiments. This lead to the development of the Coulomb testbed at the University of Colorado at Boulder, which is dedicated to Coulomb actuated relative motion studies. The testbed provides a platform to investigate charge actuation, induced and secondary affects, and environmental interactions. These are all aspects that require meticulous examination prior to space-based implementation.

The testbed features a near-frictionless one-dimensional (1D) air-bearing track with a single moving cart. Previous studies on the Coulomb testbed include closed-loop autonomous position control of the cart using electrostatics that mimic constrained orbital motions[30]. These studies identify both mechanical and electrostatic disturbances present during experiments, even though the cart motion is still dominated by Coulomb forces. To develop a deeper understanding of this implementation of Coulomb control it is necessary to understand these disturbances and develop a terrestrial Coulomb force model, taking the concept beyond the limitations of purely analytic studies.

This paper further identifies and explores the testbed disturbances present. A new Coulomb force model that incorporates close finite sphere and induced charge affects is investigated and applied to experimental results. This study on charge implementation and associated improvements on Coulomb force modelling is fundamental for terrestrial as well as space-based applications.

II. COULOMB TESTBED

The Coulomb testbed is designed and manufactured solely for exploring the implementation of charged relative motion. The Coulomb force magnitudes capable on the testbed are less than 20 mN, requiring disturbances forces to be even lower than this. With the

requirement of a low friction environment and the ability to handle unknown electrostatic interactions arose the need for a dedicated testbed. This section details the hardware apparatus and the identification of primary disturbances. Through mitigation of these disturbances an understanding of the underlying charge interactions can be achieved and the terrestrial Coulomb force model improved. This will ultimately correlate to the use of charged spacecraft formations.

II.I Hardware Apparatus

The Coulomb testbed comprises a one-dimensional air-bearing track. A rigid, low-mass cart allows motion along the 500 mm test track section. The cart and track apparatus are constructed entirely of plastic components to prevent electrostatic discharge and reduce interferences. The custom and cost-effective testbed is shown in Figure 2. Complete details on the design and manufacture of the testbed can be found in References 29 and 30.

The Coulomb force is generated by the interaction of two aluminium-coated spheres that are charged to a desired potential up to ±30 kV with electrostatic power supplies. The charged relative motion is performed by having a single sphere fixed at one end of the track and one sphere on the cart. Each sphere has a radius of 0.125 m, allowing the closest separation without discharge to be 0.3m. By manipulation of the spheres' potential, the force can be made attractive and repulsive to drive the position of the cart to a desired location.

In order to minimize airflow requirements and disturbances the testbed features an autonomous air system that supplies air only underneath the cart as it moves along the track length. For this system, an array of infrared detectors sense cart position and use hardware logic circuits to control air valves.

In order to implement autonomous feedback position control a laser is used for accurate range measurements. A central processing computer operates custom software for implementing control algorithms through the electrostatic power supplies. The software also provides a graphical user interface for user monitoring and input of testbed systems.

The cart is manufactured from polycarbonate for its dimensional stability and has a total mass (with sphere) of 0.48 kg. The charge to the moving sphere is currently provided through a fine conducting wire suspended from the above the testbed track.

II.II Testbed Coulomb Force Capabilities

In a vacuum the Coulomb force between two point charges q_A and q_B is calculated using:

$$\left|\vec{F}_c\right| = k_c \frac{|q_A q_B|}{d^2} \qquad [1]$$

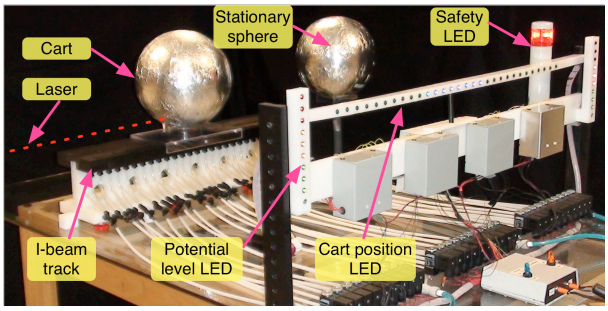

Fig. 2: Coulomb testbed providing one-dimensional relative motion control with electrostatic forces.

where k_c = 8.99x10^9 Nm^{2}C^{-2} is the vacuum Coulomb constant and d is the separation distance between the charges. If the charge is an isolated finite body modeled as a conducting sphere maintaining a fixed potential V, the resulting charge is:

$$q = \frac{Vr}{k_c} \qquad [2]$$

where r is the sphere radius. Using Equations [1] and [2] as a baseline for the testbed, the resulting force magnitude ranges from 3-20 mN over the 500 mm track length. This is computed at the full 30 kV potential and does not account for any electrostatic influences. This gives an indication of the level to which disturbances must be measured and reduced to. Providing a margin from the lowest Coulomb force level, it is desired to maintain all disturbances forces below 1 mN.

II.III Disturbances

A fundamental purpose of the testbed is to provide an environment of minimal disturbances allowing the cart motion to be dominated by the Coulomb forces. This is a difficult task given the low magnitude of electrostatic forces that can be achieved for reasonable and safe charge levels. The disturbances acting on the testbed fall under two main categories, which are explained and quantified in this section.

II.III.I Mechanical disturbances

Mechanical disturbances include undesired forces such as gravitational and air flows. The plastic track surface is machined and measured to have an overall height variation less than 0.1 mm. This is critical as a gravitational perturbation on the cart of 2 mN is reached with a local track angle of only 0.024°. The cart is also precisely mass balanced to ensure minimal centre of gravity offsets. In addition, the airflow is routinely measured and corrected along the track length at each air hole inlet to ensure even flow speeds and minimal disturbance.

Glide tests are a convenient way of measuring mechanical disturbances without the presence of electrostatics. These glide tests are performed by giving the cart an initial impulse at one end of the track and measuring the resulting acceleration profile as it travels the track length. Results of glide tests indicate that mechanical disturbances are reduced below 0.5 mN along the track length. Glide tests are performed prior to all electrostatic experiments to ensure a minimal disturbance state is reached.

With the charge cable attached to the cart there is an additional disturbance contribution. Without a charge on the cable, an additional perturbation as great as approximately 0.25 mN is minimized through appropriate attachment and length adjustment.

II.III.II Electrostatic Influences

Perturbations that are present on the cart only during Coulomb actuation are termed electrostatic influences. Isolating and measuring electrostatic influences is a non-trivial task. The utilization of electrostatics and identifying the presence of unknown charge interferences is one of the primary motivations for developing the testbed and performing Coulomb motion experiments

Depending on the conditions, charge influences have both detrimental and positive affects on cart motion and include finite sphere and induced charge affects, apparatus dielectric charge build up, and ionization and atmospheric interactions. The testbed is constructed to minimize electrostatic influences; however, since the preliminary Coulomb actuation tests, these influences have been witnessed[29].

II.IV Previous Experimental Results and Identification of Disturbances

Proof of concept experiments demonstrating electrostatic actuation on the track was performed in 2009[29]. Glide tests on this track showed disturbances as great as 10 mN. Experimental results of attractive and repulsive motions show that Coulomb forces still allowed actuation in restricted track sections. These early test offered the first identification of electrostatic discrepancies and induced motions[29].

With testbed progression, significant reductions in mechanical disturbances allow closed-loop position control experiments to be undertaken. By intentionally inclining the track, creating a known gravity bias, position control experiments are performed that mimic the constrained orbital motion of two craft aligned with the principal orbit axes[30]. While successfully controlling the cart motion, these experimental results highlight further electrostatic performance inconsistencies. The cart motion response differs between attractive and repulsive forces and potential control saturation occurred where simulations did not anticipate.

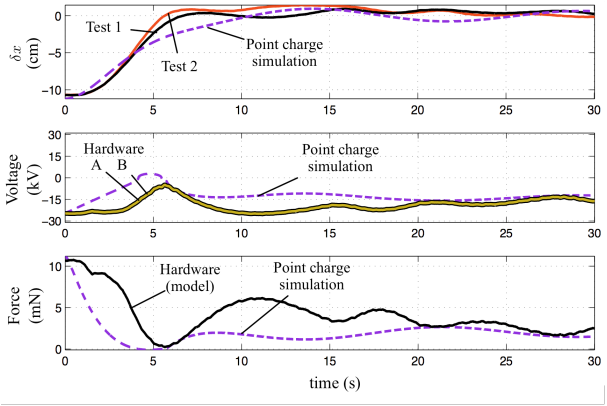

Fig. 3: Closed-loop cart position control on an intentionally inclined track, mimicking a two spacecraft out-of-plane orbit configuration.

Figure 3, adapted from previous work[30], gives an indication of the discrepancies between the system response compared to the baseline, point-charge, Coulomb force model of Equation [1].

Figure 3 shows the results of a closed-loop experiment using Coulomb forces to reposition the cart a total distance of 120 mm. The controller used is a proportional, integral, derivative (PID) controller selected for its robustness. The force model used in the controller is the baseline force model of Eq. [1]. The controller is not optimal but is implemented to investigate feedback control[30].

This test is performed on a track that is intentionally sloped up from the stationary sphere. A sloped track introduces an attractive gravity bias that is similar to the gravity gradient a pair of spacecraft aligned along the out-of-plane principal axis will experience. In this test, the cart starts next to the stationary sphere, travels up the slope away from the stationary sphere and is then held at its desired position with homogenous (repulsive) charge product.

The position of the cart from the desired location is shown in the top plot of Fig. 3 for two repeated tests as well as a simulated response with equivalent controller parameters. Glide tests on this track indicate a 2 mN gravity bias which is similarly added to the simulation. The centre plot shows the voltage output of each of the electrostatic power supplies with comparison to the simulation result. The lower plot shows the experimental and simulation force computed using the separation distance and force model of Eq. [1].

The duration of experiments performed on the testbed is typical on the order of seconds. This is necessary to allow the Coulomb forces to dominate cart motion. In contrast, spacecraft at GEO are anticipated to perform similar Coulomb manoeuvres over hours. At GEO, the Coulomb force magnitude is significantly large than the perturbations, allowing actuation to

dominate for lower control authority over longer durations. This also allows the natural orbital dynamics to assist where appropriate.

An observation of these results is that there is a reduced system response compared to the simulation model. Additionally, greater magnitude and sustained potentials are required to perform the manoeuvre. In order to continue expanding upon the applications of the testbed it is necessary to further understand the properties of electrostatic force production and improve the Coulomb testbed force model.

III. COULOMB FORCE MODEL IMPROVEMENTS

Equations 1 and 2 are used as the baseline model for Coulomb force generation on the terrestrial testbed for previous results analysis[29,30]. Figure 3 is an example of the force model's limitation on the testbed, as it does not capture all of the true electrostatic force production qualities. The aim is to improve the accuracy of the terrestrial Coulomb force model from the benchmark vacuum point-charge force given in Eq. 1. A candidate electrostatic interference function $S(r,Q,t)$ is sought that can be added to the force model resulting in an equation of the form:

$$\left|\vec{F}_{lab}\right| = k_c \frac{|Q|}{d^2} S(d,Q,t) \qquad [3]$$

where S is a model comprising of functions based on separation distance, charge product ($Q = q_A q_B$) and polarity, time (t), or a combination of each.

III.I Finite Sphere Model for Close Proximities

An improvement to the testbed force model is made by including the effect on effective charge when two finite spheres are used. This has a significant influence on the effective charge of each sphere when the centre-to-centre separation is low relative to the sphere radii (separations less than approximately 10 sphere radii, $d < 10r$). Figure 4 shows two close spheres that maintain a fixed potential, V. In the absence of sphere B the point charge of A is computed using Eq. 2. However, with sphere B reintroduced the net potential of both spheres changes the effective sphere charge and consequently the Coulomb force.

The potential at sphere A is computed including the charge of sphere B (assuming equivalent polarity) using the expression[31,32]:

$$V_A = k_c \frac{q_A}{r} + k_c \frac{q_B}{d} \qquad [4]$$

If spheres A and B are also set to the equivalent charge magnitude, $q_A = q_B$, Eq. 4 can be arranged to give an expression for the effective charge:

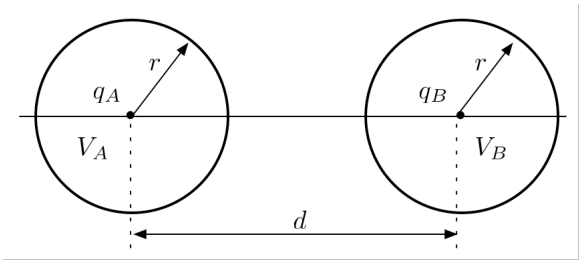

Fig. 4: Finite model for two close proximity charged spheres.

$$q_i = \frac{V_i}{k_c}\left(\frac{rd}{d+r}\right) \qquad [5]$$

If the spheres have a large separation distance ($d >> r$) Eq. 5 will reduce to the standard single sphere charge defined in Eq. 2, as required. The effective charge and Coulomb force is reduced from the equivalent point charge model for this repulsive case. If the spheres are now charged to opposite polarities (attractive force), so $q_A = - q_B$ then the effective charge is computed using:

$$q_i = \frac{V_i}{k_c}\left(\frac{rd}{d-r}\right) \qquad [6]$$

For the attractive force case, the effective charge and Coulomb force is increased from the equivalent point charge model.

III.II Close Sphere Induced Charge Models

An additional improvement to the testbed force model is the inclusion of induced charge effects that occur when the spheres are operating in very close proximity (separations less than approximately five sphere radii, $d < 5r$). When the spheres are driven to a fixed potential, but in close proximity, the charge distribution on the sphere is no longer evenly distributed[33] voiding the use of Eq. 2, which results in a discrepancy from the point charge force of Eq. 1. Two methods for computing induced charge affects are investigated and compared.

III.II.I Electrostatic Method of Images

One method of accounting for close sphere induced effects is by representing the spheres' charge with an infinite series of charges computed using the method of images[31,32,33]. Figure 5 is used as an example to highlight the principle of the electrostatic method of images. Separately, spheres A and B have a fixed potential due to each respective charge q_A and q_B located at sphere centre; however, at close separations a redistribution of charge occurs. This is modelled with a series of charges q_i, of decreasing magnitude, at decreasing separations x_i.

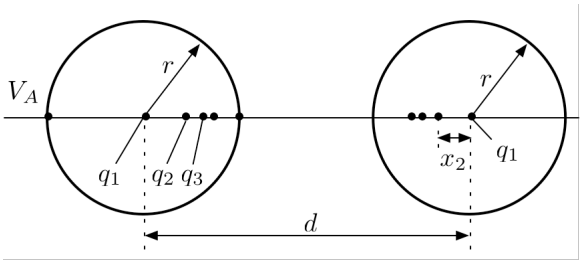

Fig. 5: Method of images to model induced charge effects of close spheres.

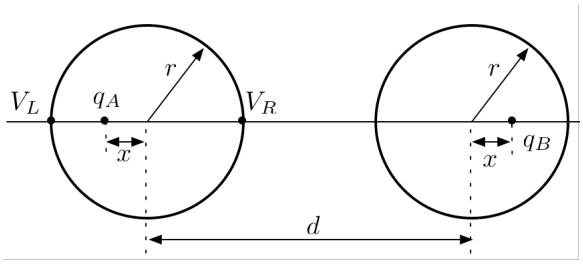

Fig. 6: First order analytic approximation to model induced charge effects of close spheres.

The values of q_i are computed for spheres of equivalent potential and polarity (repulsive force) using:

$$q_i = -\frac{rq_{n-1}}{d - x_{n-1}} \qquad [7]$$

where $n>1$, $q_1=q_A$ and $x_1=0$. This results in an overall reduced net Coulomb force. For spheres of equivalent potential but opposite polarity (attractive force), Eq. 7 is modified with a positive sign as all charges summate, increasing the effective Coulomb force. The values of x_i are computed using:

$$x_i = \frac{r^2}{d - x_{n-1}} \qquad [8]$$

where $n>1$. Numerical computation is used to calculate the ratio of charges and locations for a finite series. It is necessary to adjust the charge value to ensure the overall charge on each sphere is equal to that of the original sphere[33] (which can be the effective value for a finite sphere, computed earlier). The net Coulomb force on the spheres is computed by summating the force between each charge from within both spheres.

III.II.II First Order Analytic Approximation

An alternate and simpler model is the first order approximation shown in Fig. 6 for spheres of equivalent potential and polarity (repulsive force). This model shifts the position of each of the original charges from the sphere centre by an offset (x). This is done to maintain the potentials V_L and V_R equivalent on each sphere based on the set of equations:

$$V_L = \frac{k_c q_A}{r - x} + \frac{k_c q_B}{d + r + x} \qquad [9(a)]$$

$$V_R = \frac{k_c q_A}{r + x} + \frac{k_c q_B}{d - r + x} \qquad [9(b)]$$

Combining these two potential equations produces the equation:

$$\frac{1}{r - x} + \frac{1}{d + r + x} = \frac{1}{r + x} + \frac{1}{d - r + x} \qquad [10]$$

Rearranging Eq. 10 produces a cubic equation in x that is analytically solved. The solution selected is the practical and positive distance solution. This model also has a solution for the case with spheres of equivalent potential but opposite polarity (attractive force). In this situation the charges of each sphere are moved closer together, increasing the effective Coulomb force.

III.III Discussion on Charge Models

Each of these models can be amended to the effective Coulomb force in the form of Eq. 3. A new model that includes the effects of both finite sphere charge and induced effects is of the form:

$$\left|\vec{F}_{lab}\right| = k_c \frac{|Q^*|}{d^{*2}} \qquad [11]$$

where Q^* is the new effective charge accounting for close finite sphere influences and d^* is the new effective sphere separation accounting for the induced effects.

To quantitatively compare the contribution of each model, Fig. 7 and 8 show the coulomb force of each model along with the baseline force ('point charge') of Eq. 1. Figure 7 shows the reduction from the point charge force that occurs for homogenous charges (repulsive forces), while Fig. 8 shows the increase from the point charge force for heterogeneous charges (attractive forces). All forces are computed for the testbed setup with spheres charged to ±30 kV. The method of images model is computed using 20 charge terms and adjusted to give an overall charge using Eq. 2. Higher order terms were also investigated but offered minimal solution improvement.

In the repulsive case, with the inclusion of just the finite sphere effective charge model the Coulomb force is reduced by 50% from the baseline (Eq. 1). This comparison is made at the closest separation distance on the testbed. In the attractive case, the force increases the force by 194% from the baseline force at closest separation. Through to separations of 800 mm (6.4 radii) the effects of the close finite spheres is still significant.

The effect of just the induced charge models is also included in this comparison. The results indicate that for very close proximities the effective force with just

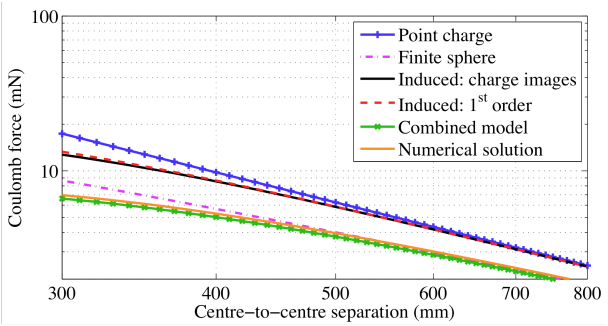

Fig. 7: Quantitative comparison of the Coulomb **repulsive** force models for testbed spheres charged to +30 kV.

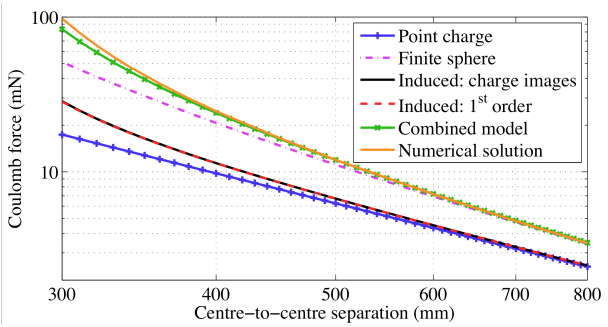

Fig. 8: Quantitative comparison of the Coulomb **attractive** force models for testbed spheres charged to ±30 kV.

induced effects decreases the force by 27% for the repulsive case and increases by 64% for the attractive case. The induced charge models also agree well with one another, and beyond a separation distance of 500 mm (4 radii) the net force effects are minimal.

The most important force calculation in this figure is the combination of finite sphere and induced charge models ('combined model' in Fig. 7). This accurately captures the true force between two closely separated charged spheres, based on Eq. 11 using the method of images to capture the induced charge influences. This combined model indicates the true repulsive force decreases by 62% from the original baseline force and the attractive force increases by 380% calculated at the testbeds closest separation.

As an additional comparison, the attractive and repulsive forces are computed for this sphere geometry numerically using Ansoft Maxwell® 13.0. These numerically solved solutions agree well with the combined model, verifying the suitability of using the new model on the Coulomb testbed.

IV. CHARGED SPHERE MODEL APPLICATION

The next step is to compare the inclusion of both the finite sphere charge and induced charge models to experimental testbed relative motion data.

IV.II Testbed Repulsion Experiment Comparison

In this study the combined model is compared to experimental data of accelerating the cart under repulsive Coulomb forces. Figure 9 shows the results of 10 sets of acceleration data from the testbed where the cart starts next to the stationary sphere and is accelerated away. The track is measured to be flat and level for these tests. Five of the tests are performed with positive 30 kV and five use negative 30 kV repulsive charges.

Each of the acceleration test results is obtained from laser range data that is differentiated twice with the data passing through a low pass filter (LPF) in each direction to remove any introduced phase lag. The cut-off frequency for the LPF is set to 0.8 Hz for this data series.

Figure 9 compares the testbed results to the equivalent acceleration capable from the point charge force of Eq. 1 as well as the new combined model of Eq. 11 that includes close finite sphere and induced charge influences. The new combined model performs well at fitting the actual testbed repulsion results.

IV.III Discussion of Model Results

The results of this testbed application shown in Fig. 9 offer three key insights. Firstly, the new and improved charge model addition significantly improves the testbed Coulomb force model and matches the testbed results well.

In addition, there are still disturbances evident in the acceleration data. This is evident particularly across the first 10 cm of the test, which shows oscillations common across all ten experimental sets.

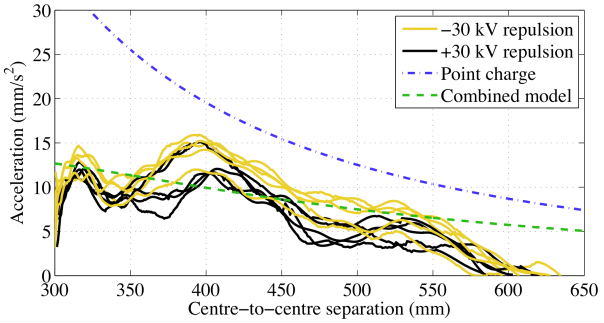

Fig. 9: Cart repulsive acceleration from stationary position comparing results for point charge and combined model at equivalent separations.

The cause for these disturbances is currently under investigation. The perturbation from the cable charging the cart's sphere is one such disturbance being quantified. While this is a very low-mass cable, any drag or disturbance is amplified during charging events when the cable stiffens under electrostatic repulsion and can induce additional oscillatory motions.

The third aspect of this data analysis that reiterates earlier work is the discrepancy between positive and negative charging repulsion. The negative charging produces a slightly larger acceleration across all separation distances. This again is a minor influence compared to the electrostatic induced effects modelled; however, this presence sheds light on the possibility of atmospheric/ionic interactions to be investigated.

V. CONCLUSIONS

The baseline point charge Coulomb force model used in previous testbed experiments lacked significant electrostatic influences. A new force model accounting for the finite sphere and induced charges of close spheres is developed. This new model is shown to fit testbed data well and is verified with numerical solution.

This new Coulomb testbed force model extends beyond the terrestrial application. The fundamental electrostatic knowledge and model influences are also applicable to the Coulomb force for spacecraft. With a new force model implemented on the testbed a significant reduction in the electrostatic influences is made allowing the investigation into further perturbations and electrostatic actuation principles.

REFERENCES

[1] Brown, O. and Eremenko, P., "Fractionated Space Architectures: A Vision for Responsive Space," 4th Responsive Space Conference, Los Angeles, CA, April 23–26 2006, Paper No. AIAA-RS-2006-1002.

[2] Gersh, J., "Architecting the Very-Large-Aperture Flux-Pinned Space Telescope: A Scalable, Modular Optical Array with High Agility and Passively Stable Orbital Dynamics," AAS/AIAA Astrodynamics Specialist Conference, Honolulu, Hawaii, Aug. 18–21 2008.

[3] Gill, E., D'Amico, S., and Montenbruck, O., "Autonomous Formation Flying for the PRISMA mission," AIAA Journal of Spacecraft and Rockets, Vol. 44, No. 3, May–June 2007, pp. 671–681.

[4] Blackwood, G., Henry, C., Serabyn, E., Dubovitsky, S., Aung, M., and Gunter, S. M., "Technology and Design of an Infrared Interferometer for the Terrestrial Planet Finder," AIAA Space 2003, Long Beach, CA, Sept. 23–25 2003, Paper No. AIAA 2003-6329.

[5] Carpenter, K. G., Schrijver, C. J., Karovska, M., and Team, S. M. C. D., "The Stellar Imager (SI) Project: A Deep Space UV/Optical Interferometer (UVOI) to Observe the Universe at 0.1 Milli-arcsec Angular Resolution," Astrophysics and Space Science, Vol. 320, No. 1-3, April 2009, pp. 217–223.

[6] Cockell, C. and et. al, "Darwin – A Mission to Detect, and Search for Life on, Extrasolar Planets," Astrobiology, Vol. 9, No. 1, 2009.

[7] King, L. B., Parker, G. G., Deshmukh, S., and Chong, J. H., "Study of Inter-spacecraft Coulomb Forces and Implications for Formation Flying," AIAA Journal of Propulsion and Power, Vol. 19, No. 3, May–June 2003, pp. 497–505.

[8] King, L. B., Parker, G. G., Deshmukh, S., and Chong, J. H., "Spacecraft Formation Flying using Inter-Vehicle Coulomb Forces," Tech. report, NASA Institute for Advanced Concepts (NIAC), January 2002.

[9] Torkar, K., Riedler, W., Escoubet, C. P., Fehringer, M., Schmidt, R., L., G. R. J., Arends, H., Rudenauer, F., Steiger, W., Narheim, B. T., Svenes, K., Torbert, R., M., A., Fazakerley, A., Goldstein, R., Olsen, R. C., Pedersen, A., Whipple, E., and Zhao, H., "Active Spacecraft Potential Control for Cluster – Implementation and First Results," Annales Geophysicae, Vol. 19, No. 10/12, 2001, pp. 1289–1302.

[10] Schmidt and et. al, "Results from active spacecraft potential control on the Geotail spacecraft," Journal of Geophysical Research, Vol. 100, No. A9, 1995, pp. 253–259.

[11] Mullen, E. G., Gussenhoven, M. S., Hardy, D. A., Aggson, T. A., and Ledley, B. G., "SCATHA Survey of High-Voltage Spacecraft Charging in Sunlight," Journal of the Geophysical Sciences, Vol. 91, No. A2, 1986, pp. 1474–1490.

[12] Whipple, E. C. and Olsen, R. C., "Importance of differential charging for controlling both natural and induced vehicle potentials on ATS-5 and ATS-6," Proceedings of the 3rd Spacecraft Charging Technology Conference, Nov. 12–14 1980, p. 887, NASA Conference Publication 2182.

[13] Lai, S. T., "An overview of electron and ion beam effects in charging and discharging of spacecraft," IEEE Transactions on Nuclear Science, Vol. 36, No. 6, Dec. 1989, pp. 2027–2032.

[14] Shuman, B. M., Cohn, H. A., Hyman, J., Robson, R. R., Santoru, J., and Willamson, W. S., "Automatic Charge Control System for Geosynchronous Satellites," Journal of Electrostatics, Vol. 20, 1987, pp. 141–154.

[15] Rustan, P., Garrett, H., and Schor, M., "High Voltages in Space: Innovation in Space Insulation," IEEE Transactions on Electrical Insulation, Vol. 28, No. 5, Oct. 1993, pp. 855–865.
[16] I. Katz, G. A. Jongeward, and et. al. "Structure of the bipolar plasma sheath generated by Spear I." Journal of Geophysical Research, 94(A2): 1450–1458, Feb. 1989.
[17] Seubert, C. R. and Schaub, H., "Tethered Coulomb Structures: Prospects and Challenges," AAS Journal of Astronautical Sciences, Vol. 57, Nos. 1-2, pp 347-368, Jan-Jun 2009.
[18] Berryman, J. and Schaub, H., "Static Equilibrium Configurations in GEO Coulomb Spacecraft Formations," AAS/AIAA Spaceflight Mechanics Meeting, Copper Moun- tain, CO, Jan. 23–27 2005, Paper No. AAS 05–104.
[19] Vasavada, H. and Schaub, H., "Analytic Solutions for Equal Mass Four-Craft Static Coulomb Formation," Journal of the Astronautical Sciences, Vol. 56, No. 1, Jan. – Mar. 2008, pp. 7–40.
[20] Natarajan, A. and Schaub, H., "Linear Dynamics and Stability Analysis of a Coulomb Tether Formation," AIAA Journal of Guidance, Control, and Dynamics, Vol. 29, No. 4, July–Aug. 2006, pp. 831–839.
[21] Wang, S. and Schaub, H., "Switched Lyapunov Function Based Coulomb Control of a Triangular 3-Vehicle Cluster," AAS/AIAA Astrodynamics Specialist Conference, Pittsburgh, PA, Aug. 9–13 2009.
[22] Wang, S. and Schaub, H., "One-Dimensional 3-Craft Coulomb Structure Control," 7th International Conference on Dynamics and Control of Systems and Structures in Space, Greenwich, London, England, July 16–20 2006, pp. 269–278.
[23] Pettazzi, L., Kruger, H., Theil, S., and Izzo, D., "Electrostatic Force for Swarm Navigation and Reconfiguration," Acta Futura, Vol. 4, 2008, pp. 80–86.
[24] Izzo, D. and Pettazzi, L., "Self-assembly of large structures in space using intersatellite Coulomb forces," 57th International Astronautical Congress, Valencia, Spain, October 2006, Paper IAC-06-C3.4/D3.4.07.
[25] Murdoch, N., Izzo, D., Bombardelli, C., Carnelli, I., Hilgers, A., and Rodgers, D., "Electrostatic Tractor for Near Earth Object Deflection," 59th International Astronautical Congress, Glasgow, Scotland, 2008, Paper IAC-08-A3.I.5.
[26] Scharf, D. P., Hadaegh, F. Y., Keim, J. A., Morfopoulos, A. C., Ahmed, A., Brenman, Y., Vafaei, A., Shields, J. F., Bergh, C. F., and Lawson, P. R., "Flight-like Ground Demonstrations of Precision Maeuvers for Spacecraft Formations," AIAA Guidance, Navigation and Control Conference, Honolulu, Hawaii, Aug. 18–21 2008, Paper No. AIAA 2008-6665.
[27] Chung, S.J., Adams, D., Miller, D. W., Lorenzini, E., and Leisawitz, D., "SPHERES Tethered Formation Flight Testbed: Advancements in Enabling NASA's SPECS Mission," SPIE – Proceedings of Astronomical Telescopes and Instrumentation Conference, Orlando, FL, 2006, Paper No. 6268-11.
[28] McCamish, S. B., Romano, M., Nolet, S., Edwards, C. M., and Miller, D. W., "Ground and Space Testing of Multiple Spacecraft Control During Close Proximity Operations," AIAA Guidance, Navigation and Control Conference, Honolulu, Hawaii, Aug. 2008.
[29] Seubert, C. R. and Schaub, H., "One-Dimensional Testbed for Coulomb Controlled Spacecraft," AAS/AIAA Spaceflight Mechanics Meeting, Savannah, GA, Feb. 8–12 2009, Paper No. AAS 09–015.
[30] Seubert, C. R. and Schaub, H., "Closed-Loop One-Dimensional Charged Relative Motion Experiments Simulating Constrained Orbital Motion," AAS/AIAA Astrodynamics Specialist Conference, Pittsburgh, PA, Aug. 9–13 2009, Paper No. AAS 09–390.
[31] Smythe, W. R., Static and Dynamic Electricity, McGraw-Hill, 3rd ed., 1968.
[32] Slisko, J. and Brito-Orta, R., "On Approximate Formulas for the Electrostatic Force Between Two Conducting Spheres," American Journal of Physics, Vol. 66, No. 4, April 1998, pp. 352–355.
[33] Soules, J. A., "Precise Calculation of the Electrostatic Force Between Charged Spheres Including Induction Effects," American Journal of Physics, Vol. 58, No. 12, Dec. 1990, pp. 1195–1199.